Dimensioning of Heliostat Components under Wind and Gravity Load: the Map Approach

Edgar Teufel[1]
Reiner Buck[1]
Andreas Pfahl[1]
Georg Böing[2]
Jens Kunert[2]

[1]German Aerospace Center (DLR), Institute of Technical Thermodynamics,
Pfaffenwaldring 38-40, D-70569 Stuttgart, Germany
Phone: +49 (0)711 6862 602, Fax: +49 (0)711 6862 747, reiner.buck@dlr.de
[2]Siemens Geared Motors GmbH, Bahnhofstr. 40-44, D-72072 Tübingen, Germany

Abstract

Estimating annual optical performance of heliostats under realistic load is computationally very expensive as complex structural deformation and ray tracing calculations are necessary. An approach is presented that vastly accelerates these calculations by using pre-calculated multidimensional maps derived from a limited number of precisely computed grid points through linear interpolation. Structural maps represent mirror misalignment as a function of wind velocity, direction and gravity. Power maps contain the intercepted power of a heliostat given its position in the field, mirror misalignment and the current sun position. The maps are generated based on specific assumptions about the tower and receiver dimensions as well as heliostat dimensions and on simple experimental investigations as for the drive properties. An estimation of the annual energy yield is obtained by integrating current intercepted power values chronologically for a given heliostat field configuration. For this purpose, representative time series for weather data (direct normal insolation, wind velocity and direction) are generated artificially. The misalignment of mirrors is calculated from wind loads taking into account wind shading effects. By applying this method to different drive configurations, the impact on the annual yield under wind loads can be rapidly identified. Thus, the method allows easy assessment of drive and other component modifications and therefore can be helpful in reducing specific costs. Results of this method are presented, using a specific heliostat design as reference. A drive train with typical stiffness properties is compared to an ideally stiff one. It is found that the method works in that it provides plausible results within reasonable computing time. Future extensions of the tool to include backlash and other drive effects are briefly described.

Keywords: heliostat, drive, wind load, weather data, annual yield, optical performance, central receiver solar tower plants

1 Introduction

Dimensioning heliostats is a challenging task. With heliostats causing roughly 45% of the costs of central receiver solar tower plants, there is much potential reward for investigating carefully how these mirrors, drives and support structures should be constructed and built. Especially the drives are relevant as they are the main cost factor with an estimated fraction of 30% of the heliostat costs [1]. One aspect about dimensioning is making sure that heliostats will withstand heavy winds. Therefore, gathering knowledge about forces and moments resulting from air flow around heliostats is essential. But there is even more to it than that. Given that a heliostat withstands storms, it might still be deflected under wind load such that part of the reflected solar radiation misses the receiver aperture. Hence, another aspect of heliostat dimensioning is reducing these spillage losses due to mirror misalignment as a result of wind-induced deformations.
Estimating wind-induced spillage losses is computationally extremely expensive as it requires both optical calculations (e.g. by ray tracing) and mechanical deformation calculations (e.g. by finite element modelling). Each of these simulations depends on many parameters and typically needs time at least in the order of minutes on current computers to evaluate single spot situations, i.e. time instants defined by heliostat and sun positions along with wind direction and speed. If one is interested in annual yield of the power plant and generally wants to gain deeper insight into the system, many time instants have to be considered – their number can easily grow up to the order of millions. Obviously, it is not possible to perform all these computations within a reasonable time frame. Therefore, an approach is presented that uses precalculated maps thus avoiding unnecessary recalculations of the optics.

2 Method overview

The basic idea behind the method is that gearbox deformations lead to mirror bias, i.e. to some erroneous alignment of the heliostat mirror frames. These mirror alignment errors or biases, one for each heliostat arm or mirror half area, can be calculated given wind speed and direction along with heliostat elevation position. Similarly, the optical performance can be calculated. For any position in a field, for any time instant (characterized by day of year and time of day) and for any mirror bias the power this heliostat would reflect into the receiver can be calculated for a specific receiver geometry and other assumptions affecting optical performance (canting method, mirror surface error, etc...). By integrating over the time steps chronologically, thereby using meteorological data for wind and insolation, an estimation of the annual yield W of one particular configuration can be obtained as follows:

$$W = \sum_{i=1}^{n} f_S(t_i)\Delta t_i \sum_{j=1}^{m} P_j(t_i). \tag{1}$$

For each time instant t_i the heliostat position (elevation and azimuth angle) are known. Current weather data for insolation and wind are also available by definition. Hence, the power currently reflected to the receiver aperture can be estimated by summing up the contributions P_j of each of the m heliostats in the field. Multiplying the resulting total power with the current time step width Δt_i and weighting it with a factor f_S representing current solar irradiation yields the energy reflected to the receiver during Δt_i. Summing up these values over all n time steps finally yields W.
The power P_j currently reflected to the receiver is affected by the wind- and gravity-induced mirror misalignment angle $\overrightarrow{\Phi}$, that mainly depends on relative wind vector $\overrightarrow{v}$ and heliostat elevation angle α. This correlation is referred to as "structural map" (see Eq. (3)).
With the current mirror misalignment angle $\overrightarrow{\Phi}$, the heliostat position in the field $\overrightarrow{r}$ and the sun position $\overrightarrow{t}$ the power P_j is defined. This correlation is referred to as "power map" (see Eq. (2)).
Both the power and the structural map consist of a number of discrete grid points at which exact calculations are carried out. Linear interpolation $L(...)$ is applied to obtain values in-between these discrete grid points. This completes the definition of the method:

$$P_j(t_i) = L(\overrightarrow{r}, \overrightarrow{t}, \overrightarrow{\Phi}), \tag{2}$$

$$\overrightarrow{\Phi} = L(\overrightarrow{v}, \alpha). \tag{3}$$

Note that power and structural maps are linked only via $\overrightarrow{\Phi}$. Therefore, they can be used independently of each other which facilitates reusing precalculated data. Wind speed and direction $\overrightarrow{v}$ as well as current direct normal insolation can be provided via a weather data file containing real data with high temporal resolution. It is assumed that the values contained in each record prevail during the whole time step Δt_i.

2.1 Heliostat power map

The time instant vector $\overrightarrow{t}$ that appears in Eq. (2) consists of two components: day of year and hour of day. Rather than specifying time with only one floating point value, this division facilitates exploiting symmetries and is better suited for linear interpolation – especially when few grid points are used. Additionally, it makes interpreting the results easier. In order to allow for assessment of configurations where mirrors are mounted to the left and right gearbox shafts without strong mechanical coupling, the mirror area has been divided into halves (left and right) and power calculations are carried out for each of them.
All power calculations can be (and have been) carried out with an extended version of the ray tracing code "MIRVAL" that was originally developed at the SANDIA labs by Leary et al. [2] in the late 70s. MIRVAL comprises a sun model capable of predicting direct solar radiation under clear-sky conditions as a function of time and site latitude/altitude [3]. By deriving a number of sun rays originating from the sun shape and tracing them until they get absorbed, hit the ground or enter into the receiver aperture, estimations of the solar power entering the receiver can be obtained. A solar power flux of 1367 W/m^2 equal to the solar constant as measured outside of the earth's atmosphere has been assumed in all power calculations to enable normalization with real insolation data (see section 2.3). The code is neither able nor intended to estimate real power yield as exact receiver and power block models are not available, but it is capable of calculating figures that can form a reliable basis for comparisons.

Note that the results are specific for the chosen receiver and heliostat configuration and can not be transferred to other power plants with different properties. Care must also be taken to ensure that the distance between grid points is not too large as this would disturb linear interpolation.

2.2 Heliostat structure map

For a given wind speed/direction $\overrightarrow{v}$ and for a given heliostat elevation angle α and mass, the wind- and gravity-induced loads on the gearbox can be calculated. As for wind loads, these can be estimated following Peterka et al. [4]. With these loads, the deformations of the gearbox shafts can be predicted for example using finite element modeling. Transforming these deformations into the azimuth-elevation coordinate system finally yields the angles $\overrightarrow{\Phi}$ at which the mirrors are misaligned, i.e. the grid points for the structural map. Equal to the case of the power map, care has to be taken to choose grid points such that linear interpolation between them does not introduce significant errors.

2.3 Integration

With precalculated structural and power maps, Eq. (1) can be applied to estimate annual yield. The weighting factor f_S for current solar irradiation can be calculated as follows:

$$f_S := \frac{S}{1367 \quad \mathrm{W/m^2}}, \tag{4}$$

with S representing the prevailing direct normal insolation as given from the weather data at time t_i. Thus, the sampled value is normalized with 1367 W/m^2, the irradiation value P_j is calculated with (see section 2.1).
As the time instant t_i also determines sun position, the exact heliostat azimuth and elevation angles, i.e. the heliostat alignment, can be calculated. With these values it is possible to determine the wind direction relative to each heliostat and look up the mirror misalignment angles $\overrightarrow{\Phi}$ in the structural map by linear interpolation. These angles are then used to look up the power the current heliostat contributes under the conditions prevailing during the current time step.
Of course most heliostats will be located in the inner part of the heliostat field. Therefore, they are not exposed to the full wind loads. Estimating how much the loads are reduced by wind shadowing is essential. Again, Peterka [4] proposes a method how this can be accomplished. He suggests to linearly reduce wind speed based on a normalized "shadow factor" that depends on the size of "upwind" mirror area in relation to the covered ground area.

3 Wind data generation

As outlined in section 2, weather data with high temporal resolution - preferably in the range of seconds - is needed to numerically solve Eq. (1) and assess the impact of wind loads on annual yield. Unfortunately, such data are not easily available as weather data records are commonly saved only every few hours or so. Thus, weather data, i.e. wind direction and speed along with solar irradiation values, have to be synthesized artificially as of now.
As for wind direction and speed, the method proposed by Shinozuka – outlined by Kaminsky et al. [5] – can be used to synthesize these data. A common choice for the spectral density of wind speed is the Davenport spectrum as summarized by Gawronski [6]. Extraterrestrial solar radiation mainly depends on the season, i.e. the current distance sun-earth, for which an approximation is available [7]. Finally, atmospheric attenuation can be roughly estimated using the correlations proposed by Hottel et al. [3] to obtain values for direct normal insolation (DNI) that are similar to measured values under clear sky conditions.

4 Application example

Trying to proof feasibility of the proposed method, a sample application on a fictional dimensioning problem is carried out. The objective is to compare a perfectly stiff heliostat gearbox structure that does not show any deformations under load at all to a gearbox with typical stiffness. The properties of an arbitrary yet typical solar tower plant are listed in Table 1.

Property	Value	Remark
Site and receiver		
Latitude	24.0° North	
Altitude	100 m	
Field extent rel. to tower	100 m East to 100 m West 200 m North to 100 m North	
Receiver height / width	2.0 m / 2.0 m	flat receiver aperture
Receiver tilt	10.0°	receiver plane tilted towards ground
Receiver azimuth angle	0.0°	receiver aperture oriented to north
Tower height	40.0 m	
Heliostats		
Facet size	3.22 m width; 1.355 m height	
Facet gap	0.015 m	
Facet columns/rows	4/7	
Heliostat mirror area	122 m^2	
Pedestial height	5.36 m	
Distance mirror surface – elevation axis	0.44 m	

Table 1. Plant properties of the fictive test case.

4.1 Power map example

For the plant and heliostat properties specified in Table 1, a power map has been created. Power calculations have been performed at ten discrete grid points equally distributed over the whole field size range. Discrete time grid points have been chosen from day 171 of the year to day 354 of the year with ten equally spaced points in between. With these days marking the summer and winter solstice respectively, and by approximatively assuming the sun position to be symmetrical in the other half of the year, the missing grid points were obtained by exploiting this symmetry. As an example it was assumed that the sun course during day 169 be equal to that during day 173. The hour of the day has been varied between 5.0 and 19.0 hours, discretised in ten steps and also distributed equally. Both azimuth and elevation mirror misalignment errors have been varied from -2.0 to 2.0 mrad in ten discrete steps of constant size, giving a total of 10^6 power calculations to build up the grid points of the optical map. As these power values can be computed independently of each other, a parallel computing approach was chosen for implementation. It took roughly three weeks to compute the optical map on a cluster of about 30 office-class PCs connected via TCP/IP. A small excerpt from the results is shown in Figure 1.
In both images a view on the virtual heliostat field in north-eastern direction is displayed (the x-axis points east).

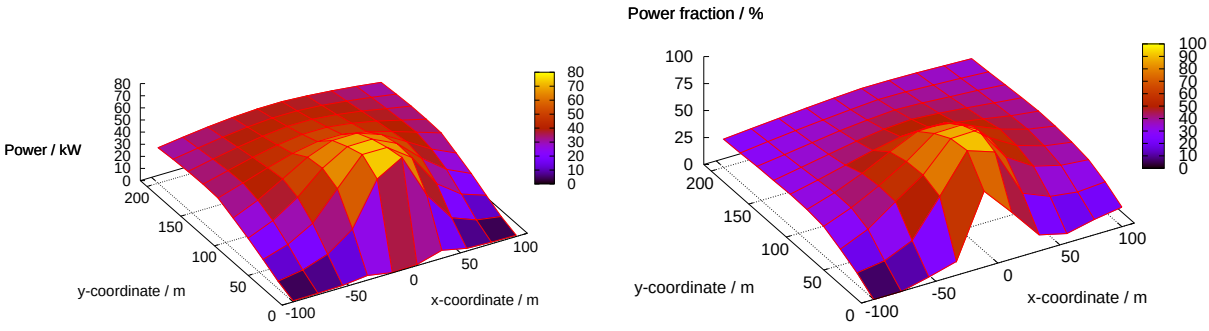

Figure 1. Power into receiver on July 26th (day 206) at 11.43h from left mirror halves: correct alignment (left) and relative difference for 2.0 mrad both azimuth and elevation misalignment (right).

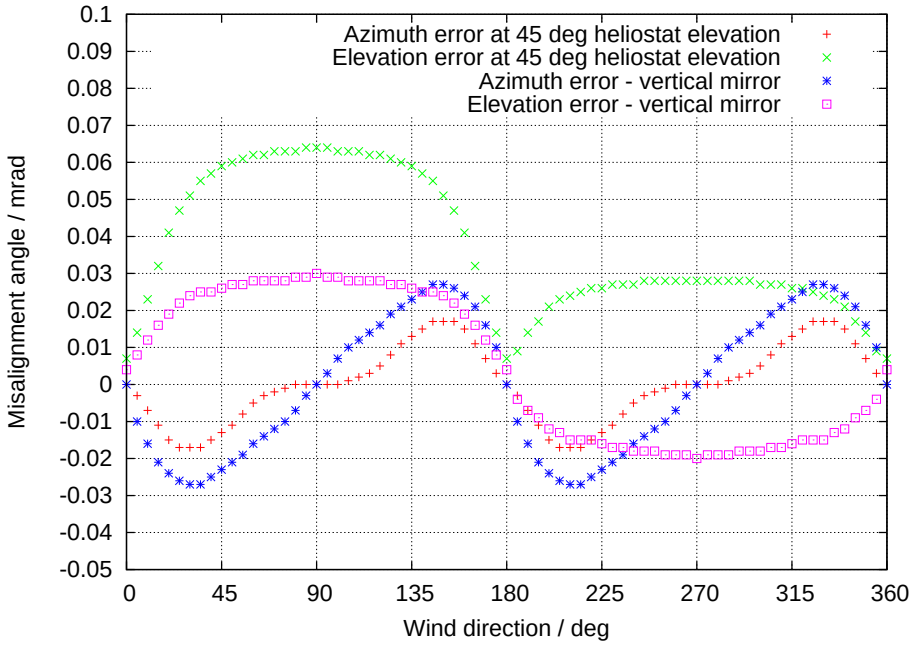

Figure 2. Mirror misalignment angle in azimuth- and elevation direction over wind direction for a mean wind speed of 4.0 m/s.

The tower receiver is located at the origin of the coordinate system. In the left part of the figure, all heliostats are aligned perfectly and the absolute power reflected into the receiver aperture is shown. In the right part all heliostats are misaligned 2.0 mrad both in azimuth and elevation direction. Here, the relative power difference to the correctly aligned heliostats is depicted. In this case, the heliostats located in the center of the field do hardly suffer from the misalignment. They still reach almost 100 % reflected power. In contrast to that, the outer heliostats do suffer considerably. Generally, the losses are higher the further the distance is. Regarding linear interpolation between the discrete grid points it can clearly be seen that grid resolution is by far high enough to suggest that linear interpolation between grid points will not introduce significant errors.

4.2 Structural map example

There is considerable choice as to where to gather mirror misalignment data from. Typically, values for mirror misalignment angles as a function of wind speed and direction would be obtained from measurements or structural deformation calculations. As the intention here is merely to assess feasibility of the proposed method, deriving the necessary data from a simplified gearbox model can be considered as both adequate and sufficient. This virtual model comprises a 0.65 m high finite element beam with a moment of inertia of $0.034 \cdot 10^{-3}\,\mathrm{m}^4$ describing the deformation of the gearbox housing under horizontal wind-induced forces. In order to model azimuth- and elevation-shaft torsion, additional beam elements are added to the model at both ends of the beam in azimuth- and elevation-direction, each having a virtual length of 0.005 m, with a polar moment of inertia of $1.1 \cdot 10^{-3}\,\mathrm{m}^4$ in azimuth- and $1.0 \cdot 10^{-3}\,\mathrm{m}^4$ in elevation-direction. Young's modulus was $210.0 \cdot 10^9$ Pa for the "housing beam" and the shear modulus was $232.0 \cdot 10^6$ Pa and $81.0 \cdot 10^6$ Pa for the azimuth- and elevation shaft respectively. All of these values are virtual as opposed to representations of real material properties. They have been adapted to match sample data collected during load deformation experiments on a real gearbox and can thus be considered realistic. Input variables of the map have been varied from zero to 20.0 m/s in ten steps, from zero to 360.0° in 72 steps and from zero to 90.0° in ten steps for wind-speed, -direction and heliostat elevation angle respectively. Heliostat properties (size of mirror area, pedestial height and mirror surface distance from elevation axes) have been chosen as outlined in Table 1. Masses were estimated to be 8600 kg for the mirrors including glass and the whole support structure and 600 kg for the gearbox itself.
Figure 2 depicts a small excerpt from the calculated map. Mirror misalignment angles for a wind speed of 4.0 m/s

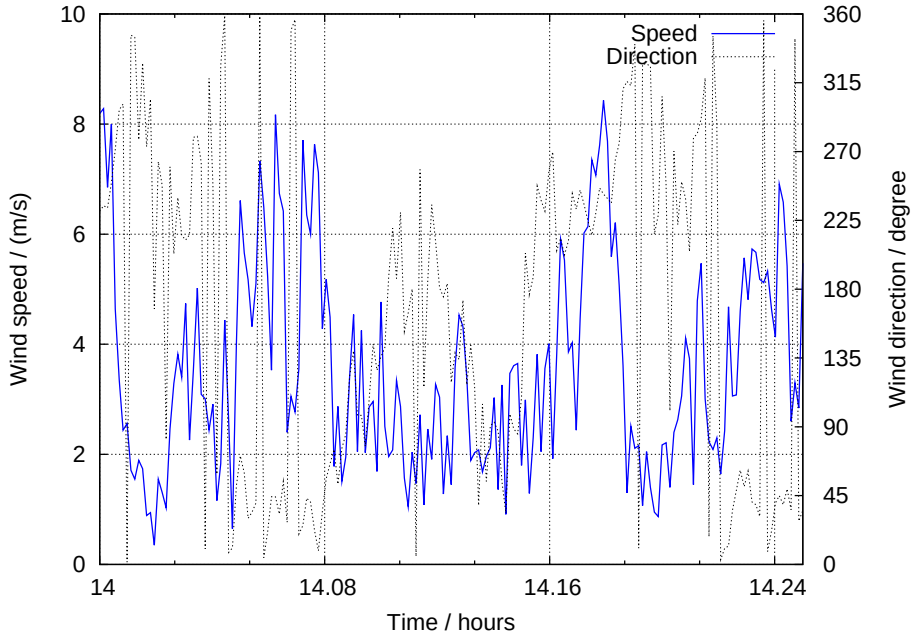

Figure 3. Synthesized data for wind direction and speed.

are shown in azimuth- and elevation direction for heliostat elevation position angles of 0° and 45°. Note how the misalignment angles around the elevation axis reach their maximum values when the wind hits the heliostat perpendicularly from the front or the back at 90° and 270° wind direction. Contrarily, the azimuth misalignment error reach their maxima for wind directions differing roughly 45° from these values. Generally, it can be seen that in this case wind load leads to a higher elevation axis alignment error, whereas the azimuth axis deformation is considerably lower overall. However, the absolute values of both errors are rather small.
Similar to the optical map example, it can again be concluded that the distance between grid points at least with respect to wind direction and heliostat elevation position is by far high enough to apply linear interpolation between these points without having to worry about introducing too much additional error.

4.3 Weather data example

For the plant properties specified in Table 1 and applying the methodology briefly mentioned in section 3, weather data have been artificially created for one year. The average wind speed was chosen to be 4.9 m/s in a reference height of 10.0 m. Terrain roughness height was assumed to be 1.0 m. One data record comprising wind speed and direction along with direct normal insolation was calculated for each five second interval. Figure 3 shows a very short time span of about 15 minutes from the synthesized wind data.
It can be clearly seen that the wind signal energy is not distributed equally over all frequencies. Instead, slow fluctuations can be distinguished from fast ones, suggesting that these wind data resemble natural behavior.

4.4 Example results

With these input data, integration runs have been carried out to solve Eq. (1) on a field with 242 heliostats. In order to save calculation time, only 91 heliostats have been taken into account for energy estimation. However, all 242 heliostats have been considered in the wind shadow calculation model. The simulated time span was one year with a temporal resolution of five seconds. Fig. 4 depicts the results for both the modeled gearbox and an ideally stiff structure that does not show any mirror misalignment due to wind loads at all. Interestingly, no significant difference between these two options can be observed, indicating that the considered gearbox does not lead to reduced annual yield when applied to heliostats and hence can be considered dimensioned sufficiently with respect to optical quality.

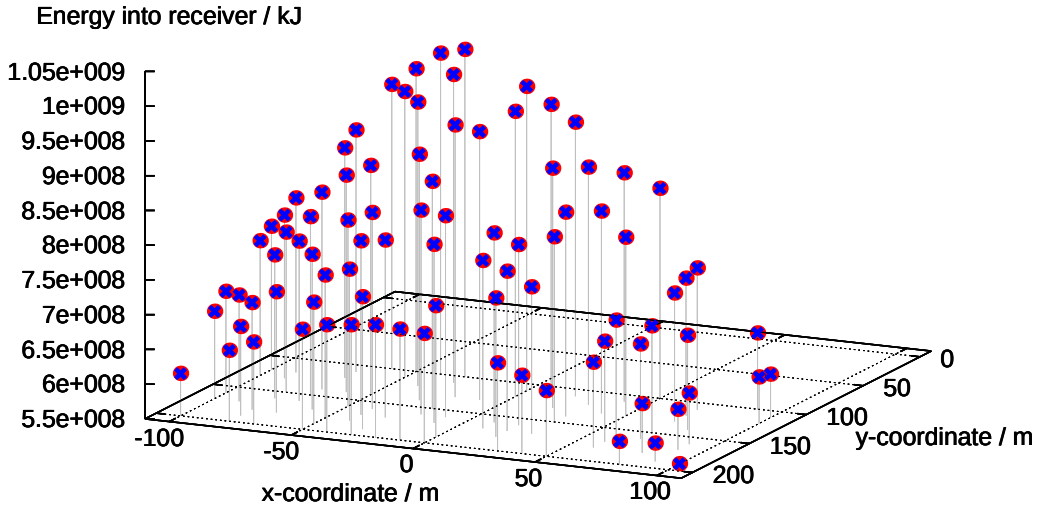

Figure 4. Comparison of annual yield of selected heliostats under wind load for perfectly aligned mirrors (red circles) and realistically misaligned mirrors (blue crosses) does not show any difference.

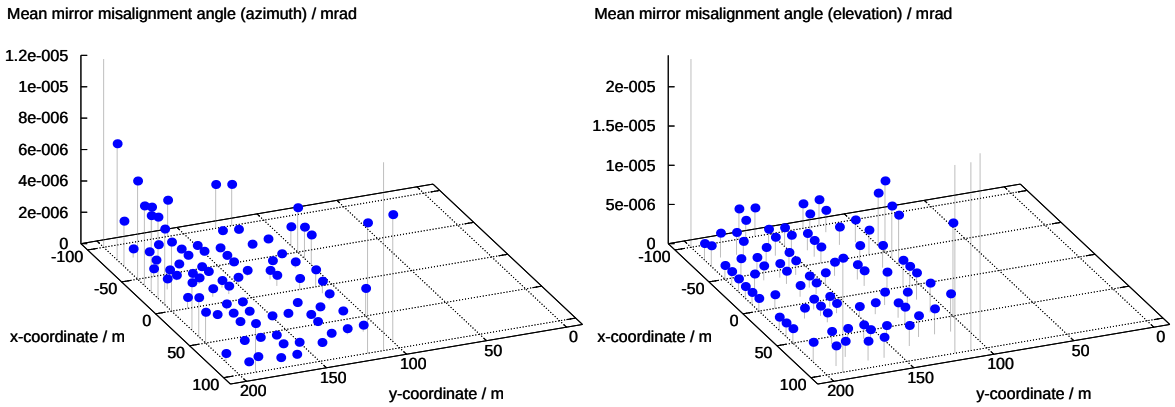

Figure 5. Average wind-induced mirror misalignment angles during the integration period: azimuth (left) and elevation (right).

Observing Figure 5, this does not come in as a surprise. This figure shows the (absolute) average mirror misalignment angles in the course of the simulation period both in azimuth and elevation direction. It can be seen that the misalignment error in elevation direction generally is higher than that in azimuth direction (note the different scales). As expected, the outer heliostats are much more prone to misalignment as the inner ones. However, and that is the most important point, the absolute values of the misalignment angles are remarkably low. With mirror surface slope errors usually being in the range of a few mrad, misalignment angle errors that are several orders of magnitude lower than that clearly will not lead to significant additional optical losses.

As for the reason for the low average mirror misalignment errors one has to consider that most heliostats are located within the field, hence in a wind-shadowed location. Additionally, wind speeds very rarely reach speeds at which significant wind loads do prevail - remember the annual average speed of only 4.9 m/s, which is a typical value. Finally, the outer heliostats tend to be operated mostly vertically, i.e. with low elevation angles. In this position, the wind induced moment around the elevation axes is low.

In sum, two integration runs are necessary to obtain results like those shown in Figure 4 - one for each gearbox construction variant. It took less than two hours to obtain annual yield data for each alternative on a modern, 1.3GHz computer with two CPU cores.

5 Summary and conclusions

Dimensioning heliostats with respect to spillage losses induced by wind and gravity loads is a challenging task that requires a lot of computational power. In this contribution, a method is described how the necessary calculations can be performed within reasonable time spans. Instead of calculating optical performance over and over again, it uses precalculated maps consisting of discrete grid points at which exact calculations have been carried out. Values between these grid points are obtained via linear interpolation.
It is found that the method delivers plausible results within acceptable time spans – if only the structural map, i.e. stiffness properties of the drive and pedestal are to be varied. Therefore, it is well suited for dimensioning these components with respect to wind and gravity loads to find a good compromise between costs and performance.
The computational effort needed to create the power map is high, yet within reach of nowadays' office-class computers.
The gearbox structure investigated in the example application proved to be stiff enough not to cause significant spillage losses due to wind-induced deflection. Hence, when solely optical performance is considered, one is tempted to draw the conclusion that it could be designed more flexible. However, this is very likely not to hold when other dimensioning aspects, e.g. dynamic strength, are also taken into account. Annual mean mirror misalignment angles turned out to be very small. This is generally in accordance with the findings in [8] where it is stated that during wind events the average wind-induced tracking error was below 1 mrad.

6 Future extensions

An important aspect of heliostat drive dimensioning is backlash. If reliable estimations about how certain amounts of backlash affect spillage losses were available, further cost reductions could most probably be achieved. Incorporating these misalignment angles into Eq. (2) is straightforward. Additional misalignment angle fractions due to backlash can simply be added to the ones originating from wind and gravity load. Moreover, the fact that backlash effects usually show hysteresis behavior which makes chronological integration a necessity does not pose an obstacle either as weather data are already synthesized as time series rather than a white noise process. Clearly, it is planned to include backlash effects in future versions of the tool. This is also expected to augment wind load induced annual yield reductions.
In order to increase reliability of results, a couple of improvements immediately come to mind. Firstly, using real weather data in the integration process rather than synthesized data sets obviously would be advantageous. Next, one would like to have the possibility to take plant operating rules like maximum wind operating speeds into account to avoid overrating of extreme weather conditions. Lastly and most importantly, revisiting the area of wind shadowing estimation could be rewarding as this affects results to a major extent.

References

[1] Thomas R. Mancini. Catalog of Solar Heliostats. SolarPACES III-1/00, Sandia National Laboratories, Albuquerque, USA, June 2000.

[2] P.L. Leary and J.D. Hankins. A User Guide for MIRVAL - A Computer Code for Comparing Designs of Heliostat-Receiver Optics for Central Receiver Solar Power Plants. Report SAND77-8280, Sandia National Laboratories, Livermore, 1979.

[3] H.C. Hottel. A simple model for estimating the transmittance of direct solar radiation through clear atmospheres. *Solar Energy*, 18:129–134, 1976.

[4] J.A. Peterka and R.G. Derickson. Wind load design methods for ground based heliostats and parabolic dish collectors. Report SAND92-7009, Sandia National Laboratories, Springfield, USA, September 1992.

[5] F.C. Kaminsky, R.H. Kirchhoff, C.Y. Syu, and J.F. Manwell. A Comparison of Alternative Approaches for the Synthetic Generation of a Wind Speed Time Series. *Journal of Solar Energy Engineering*, 113:280–289, November 1991.

[6] W. Gawronski. Three Models of Wind-Gust Disturbances for the Analysis of Antenna Pointing Accuracy. Report 42-149, California Institute of Technology, Jet Propulsion Laboratory, May 2002. IPN Progress Report.

[7] `http://solardat.uoregon.edu/SolarRadiationBasics.html`.

[8] John W. Strachan and Richard M. Houser. Testing and Evaluation of Large-Area Heliostats for Solar Thermal Applications. Report SAND92-1381, Sandia National Laboratories, Livermore, 1992.